

Flow and Thermal Characterisation of Solid Breeder Blankets with Li_2TiO_3 , Li_4SiO_4 , LiO_2 and Al_2O_3 Pebbles

Darshan C. *, Brayan Joel Pinto, Allan Loyd Fernandes, Hari Krishna V.

Department of Mechanical Engineering, St Joseph Engineering College, Mangalore, India

Abstract Lithium based ceramics such as Lithium Titanate (Li_2TiO_3), Lithium Orthosilicate (Li_4SiO_4) and Lithium Zirconate (Li_2ZrO_3) are promising solid breeder materials used in the Test Blanket Module (TBM) for the extraction of tritium. These breeders should have good thermal properties especially thermal conductivity as well as good tritium breeding characteristics. The thermal properties of tritium breeders are important for the blanket design. The tritium breeding reaction occurring in the pebble bed is an exothermic reaction liberating a large amount of heat. Thus generated heat is transmitted through the packed pebble bed. With the increase in temperature of the pebble bed the tritium breeding ratio decreases. As a result heat produced must be effectively removed from the pebble bed in order to maintain the required tritium breeding ratio. This can be achieved if the thermal conductivity and heat transfer of the packed bed is high. In this study the pebbles of Li_2TiO_3 , Li_4SiO_4 , LiO_2 and Al_2O_3 have been compared based on their flow characteristics and temperature distribution. The plot of temperature distribution shows the difference in heat transfer among the various pebbles. The simulation details and results are discussed in this paper.

Keywords Solid breeder materials, Test blanket module, Tritium, Thermal conductivity, Pebble bed

1. Introduction

ITER is an international nuclear fusion research and engineering mega project. Whose main objective is to produce electrical energy from nuclear fusion reaction. Till date thousands of engineers and scientists have contributed to the design of ITER since the idea for an international joint experiment in fusion was first launched in 1985. The ITER members—China, the European Union, India, Japan, Korea, Russia and the United States are now engaged in a 35 year collaboration to build and operate the ITER experimental device. The fossil fuels that shaped 19th and 20th century civilization can only be relied on at the cost of greenhouse gases and pollution. A new large-scale, sustainable and carbon-free form of energy is urgently needed. The following advantages make fusion worth pursuing. Fusion doesn't emit harmful toxins like carbon dioxide or other greenhouse gases into the atmosphere. Its major by-product is helium an inert and non-toxic gas. Nuclear fusion reactors produce no high activity, long-lived nuclear waste. Also there are no enriched materials in a fusion reactor like ITER that could be exploited to make nuclear weapons. And ITER lays the best platform to achieve it. Fusion reactors of the past have been able to

achieve a maximum of 16 MW of fusion power from a total input power of 24 MW ($Q=0.67$). ITER is designed to produce a ten-fold return on energy ($Q=10$), or 500 MW of fusion power from 50 MW of input power [1]. But the problems faced by ITER are the availability of the fuel deuterium (D) and tritium (T). Deuterium is a stable isotope of hydrogen which is abundantly available in sea water. Whereas tritium is an unstable isotope of hydrogen found only in traces within the earth's atmosphere and as a result it is important for us to find different methods to conserve it.

There are several methods available to produce tritium, out of which the three main methods are stated here. The first method is by using heavy water moderated reactors. But this method is not preferred as this reaction has a small neutron cross-section (probability of single neutron capture event) and also the tritium thus obtained from the separator is less and hence it is not an efficient and economical process. The second and third method used for the extraction of tritium is by using liquid and solid breeder reactors. ITER reactor is designed for both the liquid as well as solid breeder reactors. Liquid breeders employ liquid metals Li and molten salts flibe and flinabe as both tritium breeders and coolants. However, it shows also some drawbacks. In fact, besides the issues related to the magneto hydrodynamic (MHD) effects and the compatibility of liquid lead lithium alloy with structural materials, it is known that the tritium Sieverts constant in (Pb_{16}Li) is low [2]. As a consequence, a high tritium permeation rate from

* Corresponding author:
darshanc45@gmail.com (Darshan C.)

Published online at <http://journal.sapub.org/ep>

Copyright © 2017 Scientific & Academic Publishing. All Rights Reserved

the liquid metal to the primary cooling system is expected at least in absence of efficient tritium permeation barriers [3]. This aspect affects the whole blanket tritium cycle, whose main steps consist of tritium extraction from the liquid breeder and tritium removal from helium primary coolant. The third method for the extraction of tritium is by using solid breeder blankets [4-7]. Li based compounds such as lithium titanate (Li_2TiO_3), lithium orthosilicate (Li_4SiO_4), lithium oxide (LiO_2), lithium zirconate (Li_2ZrO_3), lithium aluminate (LiAlO_2), etc., known for its excellent lithium density, tritium release capability and material compatibility, is used as breeder [5], beryllium as a neutron multiplier, graphite as a reflector and RAFM Steel as a structural material. Li_4SiO_4 or Li_2TiO_3 , beryllium and graphite are used in pebble-bed forms [6]. Helium is used as a coolant and is supplied at a static pressure of 8 MPa with an inlet temperature of 300°C and an outlet temperature up to 500°C depending on the operating conditions [7]. These breeders are one of the most significant designs used in the future fusion reactors [8, 9]. In order to extract tritium from the breeder bed high energy neutrons obtained from the fusion reaction are made to strike the ceramic pebble bed made up of Li_2TiO_3 , Li_4SiO_4 , etc., which results in the formation of tritium around the pebble bed [8, 10]. The generated tritium atom in the lithium vacancy is bonded to the oxygen atoms surrounding the vacancy. The vacancy-tritium complex formation energies are in the range of 0.41-1.28 eV under oxygen rich condition [11]. Then by passing helium with 0.1-1% hydrogen as a purge gas tritium is extracted from the ceramic breeder [8]. The helium passed reacts with tritium and forms a compound with it which can later be separated and stored.

The above mentioned solid breeder materials should have good thermal properties especially thermal conductivity as well as good tritium breeding characteristics. The thermal properties of tritium breeders are important for the blanket design. The tritium breeding reaction occurring in the pebble bed is an exothermic reaction liberating a large amount of heat. Thus generated heat is transmitted through the packed pebble bed. With the increase in temperature of the pebble bed the tritium breeding ratio decreases. As a result heat produced must be effectively removed from the pebble bed in order to maintain the required tritium breeding ratio. This can be achieved if the effective thermal conductivity of the pebble bed is high, due to which the heat generated in the bed during breeding can be easily transmitted, thus helping in maintaining the desired bed temperature. Thus it is important to study the ability of the various ceramic breeders to transfer the heat through them. This study hence deals with the comparison of the various pebbles of LiO_2 , Li_4SiO_4 , Li_2TiO_3 and Alumina (Al_2O_3) based on their thermal properties i.e. their ability to effectively transfer the heat through them. It must be noted that the alumina pebble bed is considered for the purpose of comparison with the other three pebble bed materials.

2. Mathematical Model

2.1. Computational Geometry

The geometry was prepared for pebble bed with pebble size of 10mm. Figure 1 shows the overall dimensions of CFD domain with boundary conditions. Figure 2 shows mesh generation for fluid and pebble phase. The number of pebbles (N_p) in CFD domain for pebble region were calculated by using porosity technique as shown in Equation (1).

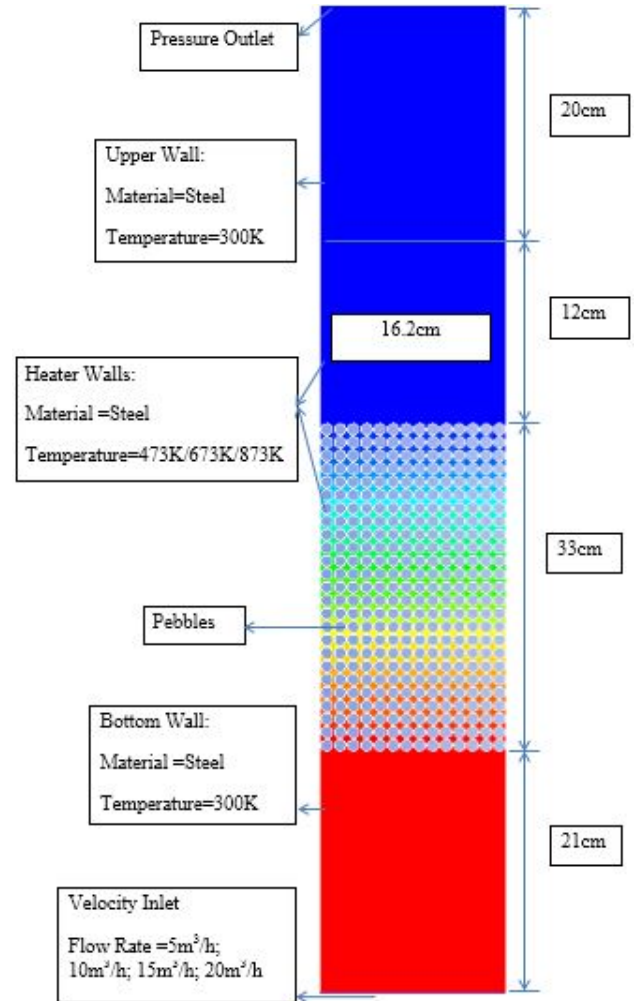


Figure 1. CFD 2D Domain and Boundary conditions

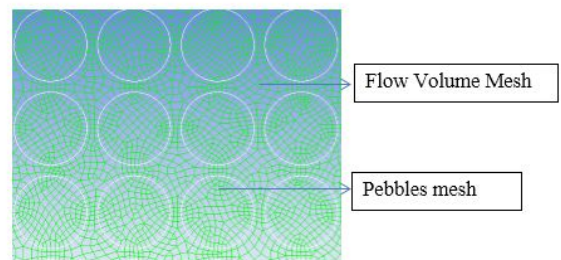


Figure 2. Mesh Generation for the Gas and Pebble Phase

$$N_p = \frac{A_b(1-\epsilon)}{A_p} \quad (1)$$

$$N_p = \frac{330 \times 162(1-0.494) \times 4}{\pi d_p^2}$$

$N_p=345$ pebbles

Where, A_b is the cross-sectional area of the bed, A_p is the surface area of one single pebble, d_p is the diameter of pebble and ϵ is the mean void fraction of bed. The value of the mean void fraction used in the present study is 0.494 for pebble bed of 10 mm pebble size.

2.2. Assumptions

- ◀ No slip boundary condition at the bed wall and at the surface of pebbles.
- ◀ Incompressible flow of air has been assumed.
- ◀ Temperature boundary condition at the bed wall is specified.
- ◀ The temperature boundary condition at the common node of pebble surface and of the fluid surface was coupled.
- ◀ User defined functions were used to define the thermal conductivity of the various pebbles and the density of air.

2.3. CFD Models

The continuity and Navier–Stokes equations [5] as shown in Equations (2) and (3) respectively were solved for laminar flow model.

2.3.1. Laminar Flow Model

The continuity and navier- stokes equations are solved for laminar flow model.

$$\frac{\partial u}{\partial x} + \frac{\partial v}{\partial y} = 0 \quad (2)$$

$$\rho_g \left(u \frac{\partial u}{\partial x} + v \frac{\partial v}{\partial y} \right) = -\frac{\partial p}{\partial x} + \mu \left(\frac{\partial^2 u}{\partial x^2} + \frac{\partial^2 u}{\partial y^2} \right) \quad (3)$$

Where ρ_g is the gas density, μ is the gas viscosity, u is the velocity along x-direction and v is the velocity along y-direction.

Equation (4) represents the energy transport equation [12].

$$\frac{\partial(\rho E)}{\partial t} + \nabla(\rho u c_p T) = \nabla(k \frac{\partial T}{\partial x}) + S_E \quad (4)$$

$$E = h - \frac{p}{\rho} + \frac{v^2}{2} \quad (5)$$

Equation ρ_g includes pressure work and kinetic energy terms which are often negligible in incompressible flows. For this reason, the pressure-based solver by default does not include the pressure work or kinetic energy when you are solving incompressible flow.

Transient term + Convection term = Conduction term + Source term

Where, ρ_g is the fluid mass density, C_p is the specific heat, k is the diffusivity and S_E is the source term.

2.3.2. k-ε Turbulent Model

The k-epsilon model is one of the most common turbulence models. It is a two equation model that means, it includes two extra transport equations to represent the turbulent properties of the flow. This allows a two equation model to account for the effects like convection and diffusion of turbulent energy. The first transported variable is turbulent kinetic energy ‘k’. The second transported variable in this case is the turbulent dissipation ‘ε’. It is the variable that determines the scale of the turbulence, whereas the first variable k, determines the energy in the turbulence. k equation and ε equation used to solve k-ε model [12] are shown in equation (6) and equation (7).

$$\frac{\partial(\rho k)}{\partial t} + \nabla(\rho k u_i) = \nabla \left(\frac{\mu_t}{\sigma_k} \nabla k \right) + 2\mu_t E_{ij} E_{ij} - \rho \epsilon \quad (6)$$

$$\frac{\partial(\rho \epsilon)}{\partial t} + \nabla(\rho \epsilon u_i) = \nabla \left(\frac{\mu_t}{\sigma_\epsilon} \nabla \epsilon \right) + C_{1\epsilon} \frac{\epsilon}{k} 2\mu_t E_{ij} E_{ij} - C_{2\epsilon} \rho \frac{\epsilon^2}{k} \quad (7)$$

Rate of change of k or ε + Transport of k or ε by convection = Transport of k or ε by diffusion + Rate of production of k or ε - Rate of destruction of k or ε.

Where, u_i represents velocity component in corresponding direction,

E_{ij} represents component of rate of deformation,

μ_t represents eddy viscosity.

$$\mu_t = \rho C_\mu \frac{k^2}{\epsilon}$$

The equation also consists of some adjustable constants $C_{1\epsilon}$, $C_{2\epsilon}$, σ_k and σ_ϵ . The values of these constants have been arrived at by numerous iterations of wide range of turbulent flows. These are as follows.

$$C_\mu = 0.09, C_{\epsilon_1} = 1.44, C_{\epsilon_2} = 1.92, \sigma_K = 1.0, \sigma_\epsilon = 1.3$$

Equation (8) shows the energy transport equation for the turbulent model [12].

$$\frac{\partial}{\partial t}(\rho E) + \nabla(\vec{v}(\rho E + p)) = \nabla \left(k_{eff} \nabla T - \sum_j h_j \vec{J}_j + (\vec{\tau}_{eff} \vec{v}) \right) + S_h \quad (8)$$

where, k_{eff} is the effective conductivity ($k_{eff}=k+k_t$, where k_t is the turbulent thermal conductivity, defined according to the turbulence model being used), and \vec{J}_j is the diffusion flux of species j. The first three terms on the right-hand side of equation (8) represent energy transfer due to conduction, species diffusion, and viscous dissipation respectively. S_h is the source term.

$$E = h - \frac{p}{\rho} + \frac{v^2}{2} \quad (9)$$

Equation (9) includes pressure work and kinetic energy terms which are often negligible in incompressible flows. For this reason, the pressure-based solver by default does not include the pressure work or kinetic energy when you are solving incompressible flow.

2.4. Pressure Drop Equations

Rate of heat transfer in pebble bed depends on the void fraction, gas flow rate, pebble and gas properties, etc. The study of hydrodynamic properties of packed pebble bed is important to understand the heat transfer process in pebble bed and the subject has been extensively studied by many investigators, as a result various correlations have been developed. Some of these correlations are discussed below. The physical properties of air, Li₂TiO₃, Li₄SiO₄, LiO₂ and Al₂O₃ used in this work are shown in Table 1.

2.4.1. Ergun Equation

Ergun Equation is commonly used to determine pressure drop across the pebble bed (ΔP_b) of height (H) at operating gas velocity, u_0 is shown in Equation (10).

$$\frac{\Delta P_b}{H} = 150 \frac{(1-\varepsilon)^2}{\varepsilon^3} \frac{\mu u_0}{\phi_s^2 d_p^2} + 1.75 \frac{(1-\varepsilon)}{\varepsilon^3} \frac{\rho_g u_0^2}{\phi_s d_p} \quad (10)$$

Where, d_p is the particle diameter, ε is the void fraction, μ is the gas viscosity, ϕ_s is the particle sphericity and ρ_g is the gas density. To use Ergun Equation to determine ΔP_b one should know the value of ϕ_s . Moreover, the accuracy of the equation lies within $\pm 20\%$. This is due to the wall effect which has not been considered in this equation.

2.4.2. Reichelt Equation

It is an equation developed by Reichelt to determine the pressure drop across the pebble bed [5].

$$\frac{\Delta P_b}{H} = K_1 A_W^2 \frac{(1-\varepsilon)^2}{\varepsilon^3} \frac{\mu u_0}{\phi_s^2 d_p^2} + B_W \frac{(1-\varepsilon)}{\varepsilon^3} \frac{\rho_g u_0^2}{\phi_s d_p} \quad (11)$$

$$A_W = 1 + \frac{2}{3(D/d_p)(1-\varepsilon)} \quad B_W = \frac{1}{[k_1(d_p/D) + k_2]^2}$$

$$K_1 = 154, k_1 = 1.5, k_2 = 0.88$$

2.4.3. Fomeny Equation

It is an equation developed by Fomeny to determine the pressure drop of packed pebble bed [5].

$$\frac{\Delta P_b}{H} = 130 \frac{(1-\varepsilon)^2}{\varepsilon^3} \frac{\mu u_0}{d_p^2} + \frac{D/d_p}{(2.28 + 0.335D/d_p)} \frac{(1-\varepsilon)}{\varepsilon^3} \frac{\rho_g u_0^2}{d_p} \quad (12)$$

Where, D is the column diameter.

2.4.4. Montillet and Comiti Equation

Equation 13 is developed by Montillet and Comiti to determine the pressure drop of packed pebble bed [5].

$$\frac{\Delta P_b}{H} = 0.061 \frac{(1-\varepsilon)}{\varepsilon^3} \left(\frac{D}{d_p} \right)^{0.2} \left[1000 \text{Re}_p^{-1} + 60 \text{Re}_p^{-0.5} + 12 \right] \frac{\rho_g u_0^2}{d_p} \quad (13)$$

Where, Re_p is the particle Reynolds number = $\frac{d_p u_0 \rho_g}{\mu}$

Table 1. Physical Properties of Air and Pebbles of Different Materials [5]

Temperature (K)	Density (kg/m ³)	Specific heat (J/kg K)	Thermal Conductivity (W/m K)	Viscosity (kg/m s)
Properties of air				
300	1.161	1,006.43	0.026	1.85x10 ⁻⁰⁵
473	0.774		0.037	2.60x10 ⁻⁰⁵
673	0.536		0.046	3.30x10 ⁻⁰⁵
873	0.409		0.052	3.30x10 ⁻⁰⁵
Properties of lithium oxide				
300	2013	1810.5	14.526	
450			10.388	
600			8.805	
750			6.618	
Properties of lithium titanate				
300	2,980	991	2.4	
450			2.0	
600			1.65	
750			1.3	
Properties of lithium orthosilicate				
300	2,000	931	1.183	
450			1.017	
900			0.921	
Properties of alumina				
300	3,975	765	36	
500			20	
800			10	

2.5. Boundary Conditions / Solution Methods / Convergence Criterion

- ◀ Inlet boundary conditions: the inlet flow is assumed at steady state condition with constant velocity profile.
- ◀ Outlet pressure: 101,325 Pa.
- ◀ The SIMPLE algorithm used for the pressure – velocity coupling with first-order upwind scheme.
- ◀ The convergence criterion was set to 1×10^{-5} for continuity equation and 1×10^{-6} for all other equations.

2.6. Grid Independence Test

The major concern while performing any kind of CFD simulation is the computational time it requires.

Computational time is directly related to the number of mesh elements i.e., if the number of elements is high then the computational time as well as the storage memory required is high. But in order to compensate for computational time if the mesh size is decreased then the accuracy will be affected. So it is important to find the optimum mesh size at which the error is minimal and the procedure incorporated to find the optimum mesh size is known as grid independence test.

Figure 3 shows the grid independence test performed on Li_2TiO_3 pebbles of 10 mm diameter at a temperature of 473 K at a radial distance of 195 mm. Five different mesh sizes have been used namely coarse, medium, fine, semi ultra-fine and ultra-fine. Table 2 shows the number of mesh elements for each type of mesh.

We can observe that the plot of coarse, medium and fine do not overlap over each other completely indicating that the accuracy of the solution still depends on the number of grid elements. But the plot of semi ultra-fine almost exactly overlap over each other. This means that with the increase in the mesh size from semi ultra-fine to ultra-fine there is no considerable effect on the temperature plot. In other words the plot of temperature becomes independent of the number of grids (meshing). Hence for the further study semi ultra-fine meshing is considered.

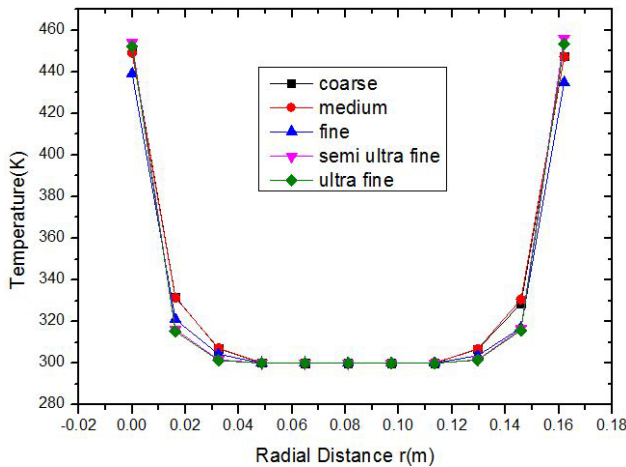


Figure 3. Grid Independence test for Li_2TiO_3 pebbles of 10mm diameter, air flow rate of $10\text{m}^3/\text{hr}$ at a bed height of $Z=95\text{mm}$

Table 2. Type of Mesh and Corresponding Number of Elements

Type of Mesh	Number of Elements
Coarse	79956
Medium	80046
Fine	80704
Semi Ultra-fine	83018
Ultra-fine	89984

3. Results and Discussions

CFD simulations were carried out for pebbles of four different materials Li_2TiO_3 , Li_4SiO_4 , LiO_2 and Al_2O_3 . The

pressure drop of Li_2TiO_3 pebbles has been plotted at 473 K at mass flow rates of 5, 10, 15 and 20 m^3/hr . The temperature distribution of the pebbles has also been plotted at 473 K/ 873 K at radial distances of 15 mm, 95 mm, 195 mm and 295 mm of the bed height.

3.1. Li_2TiO_3 Pebbles

3.1.1. Pressure Drop

Figure 4 shows the plot of bed pressure drop versus the flow rate for the pebbles of Li_2TiO_3 having a diameter of 10mm. The simulations have been carried out under laminar, k- ϵ and low Reynolds number k- ϵ model and validated against the experimental and simulation results obtained from Mandal. et. al. The plot also shows the analytical solution of pressure drop obtained from equations (10-13). It can be observed from the plot that as the mass flow rate increases the bed pressure drop increases. This occurs because as the flow rate increases the Reynolds number increases due to the increase in turbulence which resists the smooth flow of air resulting in an increase in pressure drop. The low Reynolds number k- ϵ model is said to provide better results compared to the k- ϵ model because it resolves better turbulence at wall due to the consideration of wall damping functions in the model.

3.1.2. Temperature Distribution

The plot of temperature versus radial distance for pebble bed of Li_2TiO_3 has been shown in figure 5. The plot shows the temperature distribution at wall temperature of 473 K at radial distances of 15 mm, 95 mm, 195 mm and 295 mm respectively. The results obtained from simulation have been compared and validated against the experimental results obtained from Mandel. et. al. It can be observed that the temperature profile increases with the increase in the bed height from 15 mm to 295 mm. This occurs because the point $z=295$ mm is closer to the heater walls compared to $z=15\text{mm}$.

3.2. Li_4SiO_4 Pebbles

3.2.1. Temperature Distribution

The plot of temperature versus radial distance for pebble bed of Li_4SiO_4 has been shown in figure 6. The plot shows the temperature distribution at bed wall temperature of 873 K at radial distances of 15 mm, 95 mm, 195 mm and 295 mm respectively. The trends obtained are similar to that obtained in figure 5. It can be observed that the temperature profile increases with the increase in the bed height from 15 mm to 295 mm. This occurs because the point $z=295$ mm is closer to the heater walls compared to $z=15$ mm.

3.3. LiO_2 Pebbles

3.3.1. Temperature Distribution

The plot of temperature versus radial distance for pebble bed of LiO_2 has been shown in figure 7. The plot shows the

temperature distribution at bed wall temperature of 873K at radial distances of 15 mm, 95 mm, 195 mm and 295 mm respectively. The trends obtained are similar to that obtained in figure 5. It can be observed that the temperature profile increases with the increase in the bed height from 15 mm to 295 mm. This occurs because the point $z=295$ mm is closer to the heater walls compared to $z=15$ mm.

3.4. Al_2O_3 Pebbles

3.4.1. Temperature Distribution

The plot of temperature versus radial distance for pebble bed of Al_2O_3 has been shown in figure 8. The plot shows the temperature distribution at bed wall temperature of 873 K at radial distances of 15 mm, 95 mm, 195 mm and 295 mm respectively. It can be observed that the temperature profile increases with the increase in the bed height from 15 mm to 295 mm. This occurs because the point $z=295$ mm is closer to the heater walls compared to $z=15$ mm as a result of which the temperature is found to be higher near $z=295$ mm.

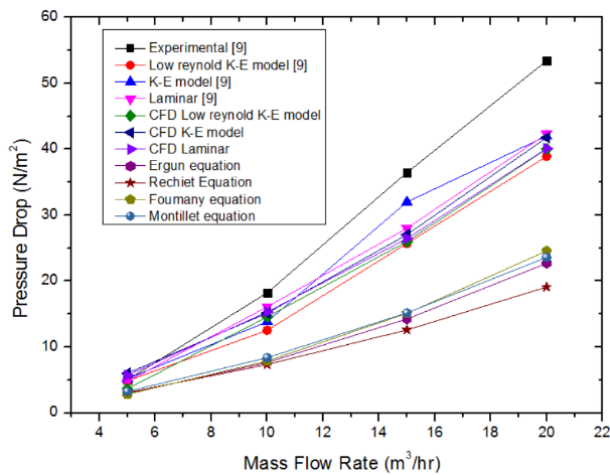


Figure 4. Variation of bed pressure drop with gas flow rate for Li_2TiO_3 pebbles (bed height: 330 mm, $D_p = 10$ mm, $\epsilon = 0.494$, $T_w = 473$ K)

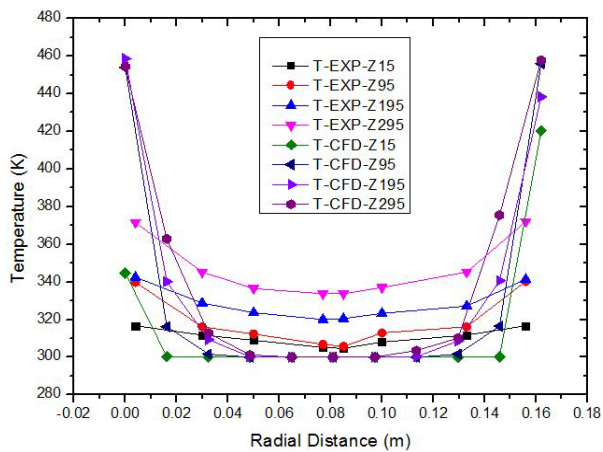


Figure 5. Variation of temperature with radial distance for Li_2TiO_3 pebbles at bed height $Z = 15$, $Z = 95$, $Z = 195$ and $Z = 295$ mm (bed height: 330 mm, $D_p = 10$ mm, $\epsilon = 0.494$, $T_w = 473$ K, air flow rate = $10 \text{ m}^3/\text{h}$)

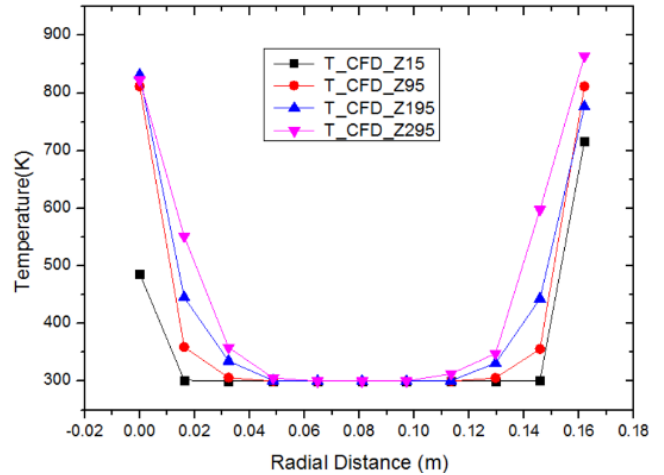


Figure 6. Variation of temperature with radial distance for Li_4SiO_4 pebbles at bed height $Z = 15$, $Z = 95$, $Z = 195$ and $Z = 295$ mm (bed height: 330 mm, $D_p = 10$ mm, $\epsilon = 0.494$, $T_w = 873$ K, air flow rate = $10 \text{ m}^3/\text{h}$)

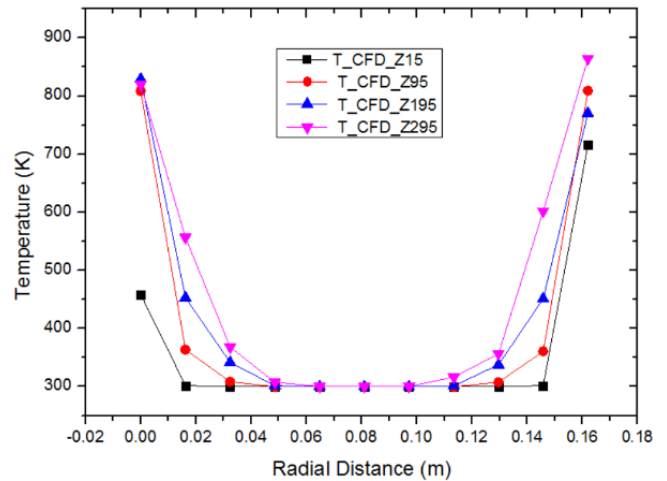


Figure 7. Variation of temperature with radial distance for Li_2O pebbles at bed height $Z = 15$, $Z = 95$, $Z = 195$ and $Z = 295$ mm (bed height: 330 mm, $D_p = 10$ mm, $\epsilon = 0.494$, $T_w = 873$ K, air flow rate = $10 \text{ m}^3/\text{h}$)

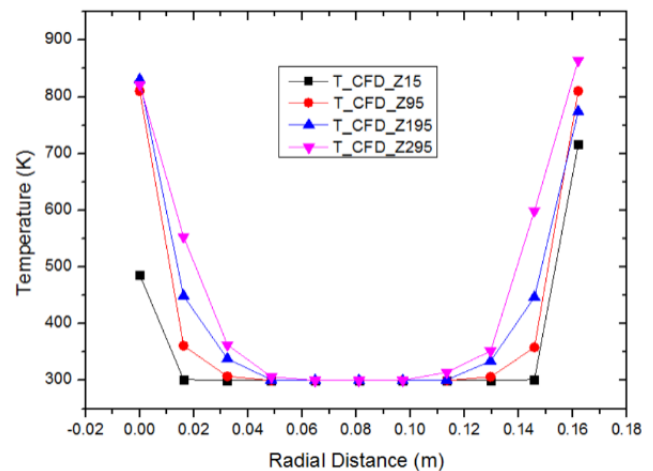


Figure 8. Variation of temperature with radial distance for Al_2O_3 pebbles at bed height $Z = 15$, $Z = 95$, $Z = 195$ and $Z = 295$ mm (bed height: 330 mm, $D_p = 10$ mm, $\epsilon = 0.494$, $T_w = 873$ K, air flow rate = $10 \text{ m}^3/\text{h}$)

3.5. Comparison of Temperature Distribution

Figure 9 shows the comparison of the temperature distribution of the pebbles of Li_2TiO_3 , Li_4SiO_4 , LiO_2 and Al_2O_3 at a bed height of 295 mm and temperature of 873 K. It can be observed that the temperature profile decreases in the order of Al_2O_3 , LiO_2 , Li_4SiO_4 and Li_2TiO_3 . The trend observed is due to the increases in thermal conductivity of the pebbles in the order of

$$\text{Al}_2\text{O}_3 > \text{LiO}_2 > \text{Li}_2\text{TiO}_3 > \text{Li}_4\text{SiO}_4$$

4. Conclusions and Future Scope

In the ITER test blanket module it is very important to achieve the tritium breeding ratio greater than one i.e., ($\text{TBR} > 1$). To obtain this ratio the heat liberated in the pebble bed during the tritium generation reaction and the heat transferred to the pebble bed from the reactor core during the fusion reaction must be extracted effectively. The thermal conductivity and heat transfer of the pebble bed play an important role in the extraction process. In this study we have compared four different pebble bed materials Li_2TiO_3 , Li_4SiO_4 , LiO_2 and Al_2O_3 from which we infer that Al_2O_3 and LiO_2 have got higher thermal conductivity and hence could be considered as a good breeder material. But it should be noted that Al_2O_3 is not a lithium based alloy (which is must for the breeder materials) and is considered for the purpose of comparison only. LiO_2 even though it is considered to be the only ceramic candidate among Li_2TiO_3 , Li_2ZrO_3 and Li_4SiO_4 for achieving the TBR larger than unity in the absence of neutron multiplier. But however, at temperatures below a moisture pressure dependent critical value (e.g. 366°C at 10 Pa), LiOH will precipitate out as a separate phase, thereby increasing tritium retention to unacceptable levels which is undesirable. Whereas both Li_2TiO_3 and Li_4SiO_4 are preferred as tritium breeding materials even though their thermal conductivities are lesser compared to LiO_2 . Since they do not produce long-lived products during the irradiation process and also they have good lithium atom density. Between Li_2TiO_3 and Li_4SiO_4 , Li_2TiO_3 holds the upper hand because it is a low activation ceramic material, its thermal stability is higher, it has got higher chemical stability and mechanical resistance also its reaction to moisture is less and has better compatibility with structural materials.

Therefore from this study we infer that thermal conductivity is not the only factor for the selection of tritium breeders. But there are also other factors like lithium atom density, affinity of pebbles towards moisture and stability to be taken into consideration while designing the pebble bed.

The major concern faced by ITER is the extraction of tritium. To sustain the reaction in the tokamak a TBR greater than one is necessary. Various breeder materials have been chosen for this purpose like Li_2TiO_3 , Li_4SiO_4 , and Li_2ZrO_3 etc. From this study we infer that Li_2TiO_3 is preferred as a suitable breeding material. In the extraction process high energy neutrons obtained from the fusion reaction are made to strike the ceramic pebble bed which results in the

formation of tritium in the bed. Tritium is then extracted by passing helium as a purge gas. The phenomenon such as diffusion, absorption and desorption are involved in this process. It is of utmost interest to calculate the amount of tritium that can be extracted by passing a known quantity of purge gas and to study the factors which influence the tritium extraction process.

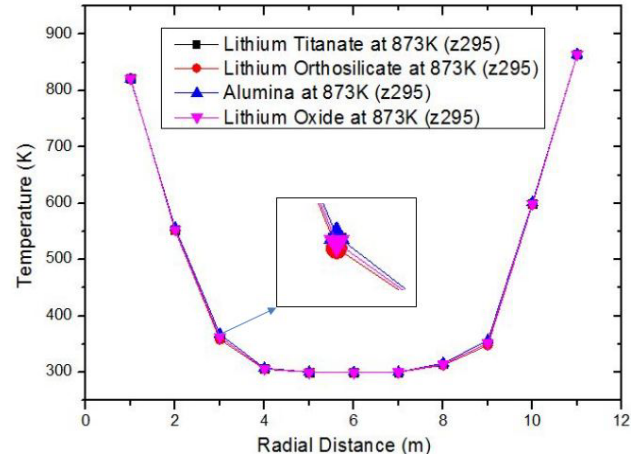


Figure 9. Variation of temperature with radial distance for pebbles of Li_2TiO_3 , Li_4SiO_4 , LiO_2 and Al_2O_3 at bed height of $Z = 295$ mm (bed height: 330 mm, $D_p = 10$ mm, $\varepsilon = 0.494$, $T_w = 873$ K, air flow rate = 10 m³/h)

Nomenclature

- A_b Cross-sectional area of bed [m²]
- A_p Surface area of a single pebble [m²]
- $C_{1\varepsilon}$ Model parameter in $k - \varepsilon$ model
- $C_{2\varepsilon}$ Model parameter in $k - \varepsilon$ model
- C_μ Model parameter for $k - \varepsilon$ model
- D Column or bed diameter [m]
- C_p Heat capacity [J kg⁻¹ K⁻¹]
- d_p / D_p Particle (pebble) diameter [m]
- g Acceleration due to gravity [m s⁻²]
- u_0 Operating gas velocity [m s⁻¹]
- h Heat transfer coefficient [W m⁻² K⁻¹]
- k Thermal conductivity of the bed [W m⁻¹ K⁻¹]
- k_{eff} Effective thermal conductivity of pebble bed [W m⁻¹ K⁻¹]
- k_g Gas thermal conductivity of [W m⁻¹ K⁻¹]
- H Length or height of bed [m]
- N_p Number of pebbles in a domain
- R_{ep} Particle Reynolds number
- T Temperature [K]
- u, v Velocity component in X & Y direction [ms⁻¹]

Greek Letters

- ε Mean void fraction
- μ Viscosity of gas [kg m⁻¹ s⁻¹]
- ρ_g Density of gas [kg m⁻³]
- ρ_s Density of pebbles [kg m⁻³]
- ΔP_b Bed pressure drop [N m⁻²]

REFERENCES

- [1] www.iter.org.
- [2] Ricapito, L.V. Boccaccini, P. Calderoni, A. Ciampichetti, D. Demange, Y. Poitevin (Tritium management in the European test blanket Systems and extrapolation to DEMO) Fusion Energy Conf., San Diego, Calif. (2012).
- [3] S. Fukada, T. Muneoka, M. Kinjyo, R. Yoshimura, K. Katayama (Hydrogen transfer in Pb–Li forced convection flow with permeable wall) Fusion Engineering and Design (2015) p 95–100.
- [4] J. Cheng, Y. Wu, W. Tian, G. Su, S. Qiu (Neutronics and thermo-hydraulic design of supercritical-water cooled solid breeder TBM). Fusion Engineering and Design (2015) p 52–58.
- [5] N.S. Ghuge & D. Mandal (CFD Analysis for the Hydrodynamics and Heat Transfer in Packed Pebble Bed) Indian Chemical Engineer © 2015 Indian Institute of Chemical Engineers (2015), p 1–23.
- [6] R. Frano, D. Aquaro, L. Scaletti (Thermo-mechanical characterization of ceramic pebbles for breeding Blanket) Fusion Engineering and Design (2016) p xxx-xxx.
- [7] G. Zhou, M. Li, Q. Liu, S. Wang, H. Chen, M. Ye (Thermal Analysis of Breeder Unit for Helium Cooled Solid Breeder Blanket of Chinese Fusion Engineering Test Reactor). Fusion Energy (2015) p 339–345.
- [8] S. Choa, M. Ahna, D. H. Kima, E. S. Leea, S. Yunb, N. Z. Cho, K. J. Junga (Current status of design and analysis of Korean Helium-Cooled Solid Breeder Test Blanket Module). Fusion Engineering and Design (2008) p 1163–1168.
- [9] D. Carloni, L.V. Boccaccini, F. Franza, S. Kecskes (Requirements for helium cooled pebble bed blanket and R&D activities) Fusion Engineering and Design (2014) p 1341–1345.
- [10] Katsui, Y. Katoh, A. Hasegawa, M. Shimada, Y. Hatano, T. Hinoki, S. Nogami, T. Tanaka, S. Nagata, T. Shikama (Tritium trapping in silicon carbide in contact with solid breeder under high flux isotope reactor irradiation) Journal of Nuclear Materials (2013) p 497–500.
- [11] Y. Shi, T. Lu, T. Gao, X. Xiang, Q. Zhang, X. Yu, Y. Gong, M. Yang (Density functional study of lithium vacancy in Li_4SiO_4 : Trapping of tritium and helium) Journal of Nuclear Materials (2015) p 519-526.
- [12] ANSYS Fluent.